

Lagrangian Chaos in a Micro Serpentine Mixer for Immunomagnetic Cell Sorting

Koji Fukagata *, Nobuhide Kasagi, and Chainarong Chaktranond

Department of Mechanical Engineering, The University of Tokyo, Hongo 7-3-1, Bunkyo-ku, Tokyo 113-8656, Japan
(October 1, 2004)

Lagrangian particle tracking simulation is performed to investigate the motion and mixing of cells and immunomagnetic beads suspended in a buffer fluid flow introduced into a micro serpentine mixer. Distributed external magnetic fields, which vary periodically in space and time, are applied in order to drive the magnetic beads in a chaotic manner and to enhance mixing. Influence of the magnetic forcing conditions, i.e., the amplitude and frequency, on the performance of mixer is examined.

I. INTRODUCTION

In regenerative medicine, it is often required to extract certain kinds of cells from a sample mixture, e.g., mesenchymal stem cells from blood or bone marrow. One of the efficient techniques for this extraction is the use of magnetic beads coated with the antibody corresponding to the antigen of the target cells.¹ This technique is called as immunomagnetic cell sorting (IMCS) and the principle and procedure of separation is shown in Fig. 1. In the first mixing process, magnetic beads coated with an antibody (i.e., immunomagnetic beads) attach the target cells that have the corresponding antigen. After the mixing, only the cells attached by the beads can be isolated from the mixture by using magnetic forces in a separator. One of the problems in the conventional IMCS equipment is the need of large amount of sample, say on the order of 1 liter, and high operation cost. A very small IMCS device, which has a potential to reduce the sample, cost, and possible infection, is therefore needed and currently under intensive study.

A key issue for successful development of such a micro IMCS device is how to achieve effective mixing of beads and cells in a flow of buffer fluid under a low-Reynolds-number environment. To resolve this, two different strategies have been proposed. One is passive mixing, which uses conduits of complex two- or three-dimensional geometry.²⁻⁴ The other is active mixing, which uses external forcing, such as pressure perturbations,^{5,6} dielectrophoretic forces,⁷ and magnetic forces.⁸ Generally speaking, passive mixer does not need additional energy so that the system would be simpler, whilst active mixer offers higher performance within a smaller space. In many cases, these are designed to enhance the mixing by utilizing so-called the Lagrangian chaos.⁹

In order to optimize the design of such micro mixing devices, effects of the design parameters on the mixing performance should be investigated. For that purpose, numerical simulation has a merit because systematic assessment can be easily made with different values of design conditions. Therefore, the objective of the present study is to numerically inves-

tigate the performance of an active immunomagnetic mixer under different operating conditions. Here, we consider the magnetic mixer of Suzuki et al.⁸ and perform Lagrangian particle tracking simulations of the motion of magnetic beads and cells in this mixer.

II. MICRO IMMUNOMAGNETIC MIXER

We consider an micro immunomagnetic mixer proposed by Suzuki et al.,⁸ as shown in Fig 2. Plane and side views of one mixer unit are shown in Fig. 3. The length and the width are L_x and L_y , and their directions are denoted as x and y , respectively. The out-of-plane direction is denoted as z and the height is L_z . Two obstacles are placed at $(L_x/8 \leq x \leq L_x/4, L_y/2 \leq y \leq L_y)$ and $(5L_x/8 \leq x \leq 3L_x/4, 0 \leq y \leq L_y/2)$ to make the conduit in a serpentine shape.

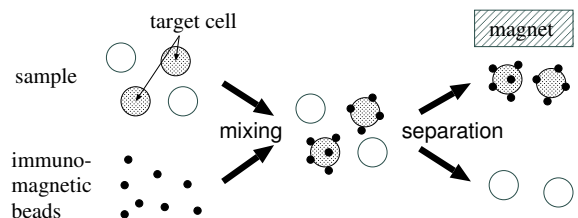


FIG. 1. Schematic of the immunomagnetic cell sorting.

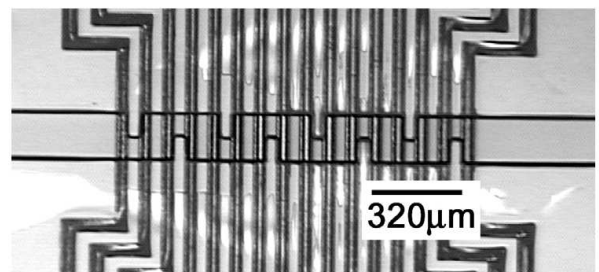


FIG. 2. Micro serpentine immunomagnetic mixer developed by Suzuki et al. (2004).

* E-mail: fukagata@thtlab.t.u-tokyo.ac.jp (K. Fukagata)

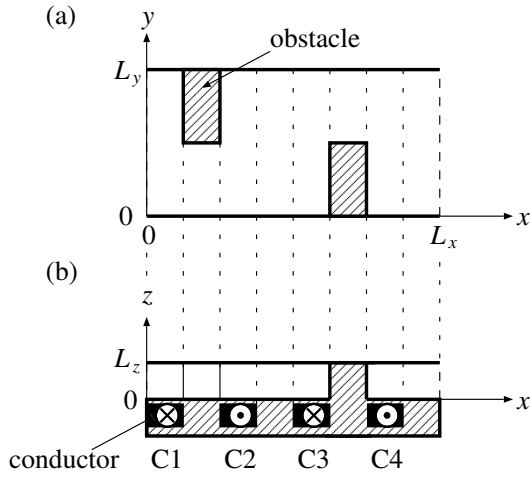


FIG. 3. Geometry of the micro mixer by Suzuki et al. (2004): (a) plane view; (b) side view. Symbols in the conductors represent the directions of positive current.

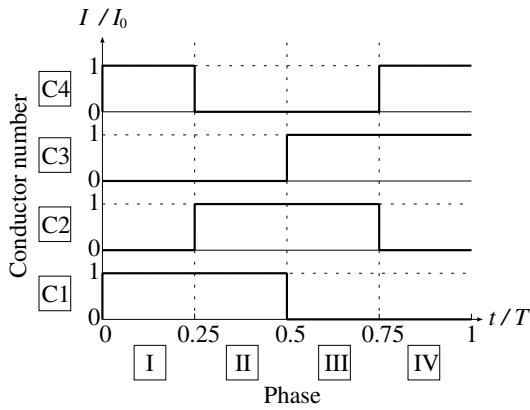


FIG. 4. Operation diagram of electric current.

Four parallel magnetic conductors (labeled as C1 through C4 in Fig. 3), of which width is $L_x/8$, are embedded with equal spacing ($L_x/4$) in the bottom wall. A counter electric current is imposed on a pair of neighboring conductors to generate a magnetic force field around them. The current is sequentially switched on ($I = I_0$) and off ($I = 0$) with a period of T , as shown in Fig. 4. As also shown in the figure, these four phases in one period are called as Phases I to IV. The Strouhal number of the magnetic actuation, St , is defined by using the period of magnetic actuation, T , and the conductor spacing, $L_x/4$, as,

$$St = \frac{(1/T)(L_x/4)}{U_b} = \frac{L_x}{4U_b T}. \quad (1)$$

Suzuki et al.⁸ fabricated, by using microelectromechanical systems (MEMS) techniques, two kinds of mixers of different sizes. The mixer is composed of a series of mixer units connected each other. The two sizes of a unit are $(L_x, L_y, L_z) = (160 \mu\text{m}, 80 \mu\text{m}, 35 \mu\text{m})$ and $(L_x, L_y, L_z) =$

$(320 \mu\text{m}, 160 \mu\text{m}, 35 \mu\text{m})$. In their experiment, a buffer fluid containing immunomagnetic beads was introduced in the upper half of the conduit ($L_y/2 \leq y \leq L_y$), whereas a pure buffer fluid was introduced in the lower half.

III. NUMERICAL PROCEDURE

An iso-thermal, incompressible water flow is considered. Throughout this work, the bulk mean velocity of the flow, U_b is on the order of $100 \mu\text{m/s}$. Therefore, the bulk Reynolds number of the flow, $Re_b = U_b L_y / \nu$, is on the order of 1×10^{-2} , so that the flow is laminar. The velocity field is computed by using the second-order accurate finite difference method on an equi-spaced grid system.

The trajectories of immunomagnetic beads and cells are computed by using the one-way coupling Lagrangian particle tracking. We assume, for simplicity, that both beads and cells (referred hereafter as particles, unless specified) are rigid spheres of $1 \mu\text{m}$ in diameter, although in reality cells are deformable and their typical diameters is on the order of $d_p \sim 10 \mu\text{m}$. The density of the beads is $\rho_p = 1580 \text{ kg/m}^3$. The relaxation time of beads, $\tau_p = d_p^2 S / (18\nu)$ (where $S = \rho_p / \rho_f$ is the density ratio of particle to fluid) is on order of $\tau_p \sim 1 \times 10^{-7}$. Thus, the simplified particle equation of motion reads,

$$\frac{d\vec{u}_p}{dt} = \frac{1}{\tau_p}(\vec{u}_f - \vec{u}_p) + \frac{\vec{F}}{m_p} - \left(1 - \frac{1}{S}\right)g\vec{e}_z, \quad (2)$$

where \vec{u}_p and \vec{u}_f are particle and fluid velocities, respectively. The last two terms in the particle equation of motion represents the external forces, i.e., the magnetic force induced by the conductors embedded under the conduit, \vec{F} , and the gravitational force. Note that the Brownian force, the inter-particle collisions and the two-way coupling effects are neglected for simplicity.

The magnetic field in the conduit, \vec{H} , is computed by using the Biot-Savart law, which reads

$$\vec{H}(\vec{x}) = \int_{\vec{x}' \in \Omega} \frac{\vec{I}(\vec{x}') \times (\vec{x} - \vec{x}')}{2\pi|\vec{x} - \vec{x}'|^2} d\Omega, \quad (3)$$

where \vec{I} is the current vector. The integration is done over the volume of conductors, Ω , which are assumed infinitely long in the y direction.

The magnetic force acting on an immunomagnetic bead is computed by

$$\vec{F} = \mu_0 \mu_r (1 - N_d) V_m (\vec{H} \cdot \vec{\nabla}) \vec{H}, \quad (4)$$

where μ_0 is the permeability in vacuum, and μ_r , V_m and N_d are the relative permeability, the volume, and the demagnetizing factor of the beads, respectively. Following the experiment,⁸ spherical beads of carboxyl-polystyrene ($\mu_r = 11.3$, $N_d = 0.333$) are assumed.

The non-dimensional amplitude of the magnetic force, α (the amplitude factor), is defined as,

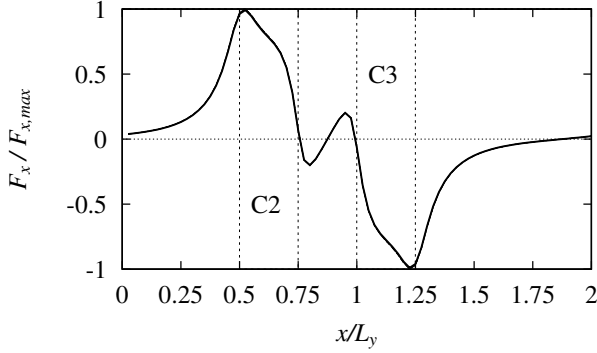


FIG. 5. Nondimensionalized magnetic force (Phase III).

$$\alpha = \frac{u_{max}}{U_b}, \quad (5)$$

where u_{max} is the terminal velocity due to the maximum magnetic force, F_{max} , i.e.,

$$u_{max} = \tau_p \frac{F_{max}}{m_p}. \quad (6)$$

It is obvious from the definition that the amplitude factor, α , expresses the relative magnitude of magnetic-force-induced particle velocity to the fluid velocity.

The particle equation of motion, Eq. (2), is stiff due to the small value of τ_p . Therefore, it is integrated in time by using the implicit Euler method. The fluid velocity and the magnetic field at a particle position are interpolated from the neighboring grid points by using the linear interpolation scheme.

IV. RESULTS

A. Two-dimensional simulation

We begin with simulations of particle motion in a $(x-y)$ two-dimensional plane.

The dimension of the two-dimensional conduit is $(L_x, L_y) = (160 \mu\text{m}, 80 \mu\text{m})$. The computational domain is periodic at both ends ($x = 0$ and $x = L_x = 2L_y$). The numbers of computational grids are 80 and 40 in the x and y directions, respectively. The bulk Reynolds number is $Re_b = 0.0032$. For the computation of the magnetic fields imposed, the computational plane is assumed to represent that located at $5 \mu\text{m}$ above the bottom wall, because Suzuki et al.⁸ observed in their experiment that the magnetic beads are accumulated in a thin layer of $0 < z < 5 \mu\text{m}$. As an example, the profile of the non-dimensional magnetic force exerted on the beads in Phase III is depicted in Fig. 5.

Figure 6 shows a typical effect of the magnetic actuation in the present mixer. The beads are initially distributed uniformly in the upper half of the conduit. Without the magnetic actuation (see Fig 6a), the beads remain in the upper half even after sufficiently long time. There is no bead which travels across the streamlines. With the magnetic actuation at the amplitude factor of $\alpha = 0.55$ and the Strouhal number of $St = 1.0$ (Fig 6b), the beads are stirred and mixed in the entire domain.

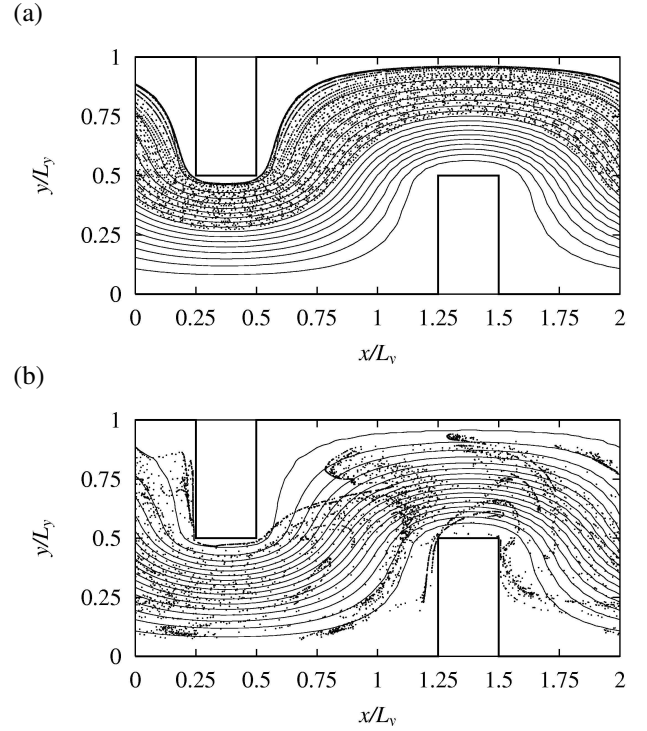


FIG. 6. Positions of magnetic beads after a long time: (a) without magnetic actuation; (b) with magnetic actuation ($\alpha = 1.55$, $St = 1.0$). Lines represent the streamlines of fluid.

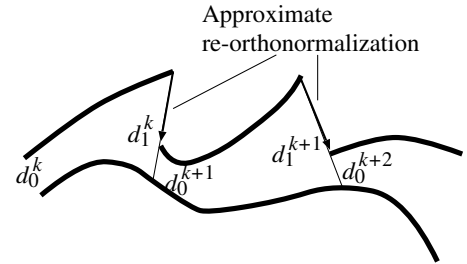


FIG. 7. Schematic of the procedure to compute the largest Lyapunov exponent.

In order to quantitatively discuss on the mixing enhancement by this scheme of magnetic actuation, the following two indices are computed:

- **Largest Lyapunov exponent, λ_1 .** The largest Lyapunov exponent, λ_1 , is the largest one in the spectrum of Lyapunov exponents, i.e., $\lambda_1 > \lambda_2 > \dots > \lambda_n$ (where n is the size of dimensions). This quantity is often used to measure the degree of chaos. If $\lambda_1 > 0$ the flow is regarded as chaotic. For the computation of λ_1 , we adopt the simplified method proposed by Sprott,¹⁰ as shown in Fig. 7. First, particles are distributed in the conduit. For each particle, an imaginary particle is placed within an infinitesimal distance (d_0). Then, the trajectories of these particles are tracked. When the distance, $d_1(t)$, between real and imaginary particles becomes far apart,

the approximate re-orthonormalization is performed by pulling back the imaginary particle along the line of separation to re-define d_0 . Namely, λ_1 is to be computed by

$$\lambda_1 = \lim_{n \rightarrow \infty} \frac{1}{n\Delta t} \sum_{k=1}^n \ln \left(\frac{d_1^k}{d_0^k} \right). \quad (7)$$

It is known that this simplified procedure gives a sufficiently accurate value of λ_1 .

- **Ratio of the number of tagged cells to the total number of cells.** This quantity is computed in a computational domain with the inflow and outflow boundary conditions. Multiple mixer units are connected to each other, like in the experimentally tested device.⁸ Nine units are used in the present simulation. The magnetic beads and cells are introduced in the upper and lower halves of the first unit, respectively. The magnetic actuation is applied in the regions from the fourth to eighth units. When the distance between a magnetic bead and a cell becomes less than the sum of their radii, the cell is considered *tagged*. The number of such tagged cells, N_{tagged} , as well as the total number of cells, N_{total} , is counted at the outlet. Their ratio, γ , is simply defined as

$$\gamma = \frac{N_{tagged}}{N_{total}}. \quad (8)$$

In the present simulation, we allow the cells to be tagged by multiple magnetic beads.

Figure 8 shows the dependency of λ_1 on the actuation parameters, α and St . In the cases of small amplitudes ($\alpha \leq 1.00$), λ_1 is always positive, and this fact means that chaotic mixing is induced. The best mixing is achieved when $St = 1.0$ and $\alpha \leq 1.55$.

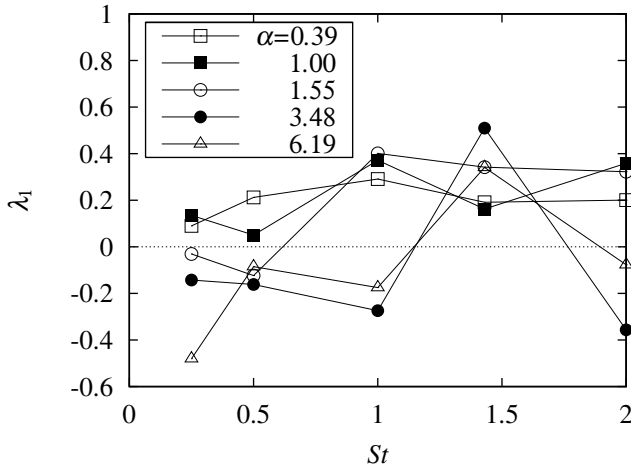


FIG. 8. Dependency of the largest Lyapunov exponent, λ_1 , on the actuation parameters, α and St .

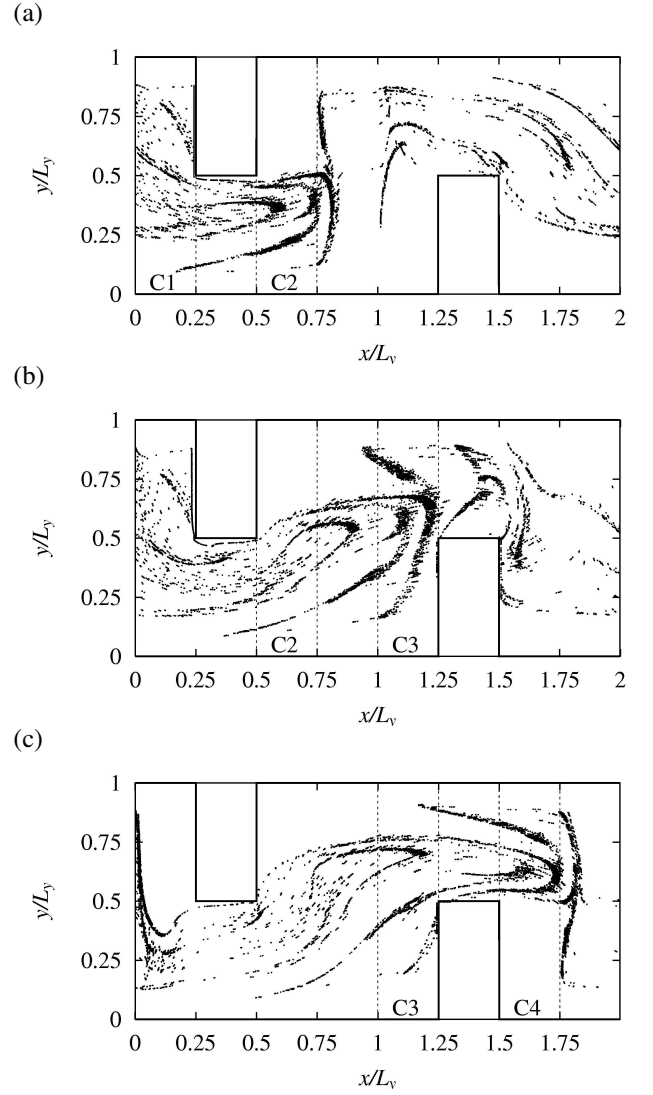


FIG. 9. Positions of magnetic beads in each actuation phase at $\alpha = 3.48$ and $St = 1.0$: (a) Phase II; (b) Phase III; (c) Phase IV. Areas enclosed by dashed lines represent the active conductors.

In the cases of large amplitude ($\alpha \geq 1.55$), λ_1 is positive only at $St = 1.4$ and is negative for other values of St . The negative values of λ_1 indicate that the magnetic beads are accumulated in certain regions. In such cases, they are trapped near the conductors. For example, the positions of magnetic beads in each actuation phase at $\alpha = 3.48$ and $St = 1.0$ (i.e., the case of $\lambda_1 < 0$) are shown in Fig. 9. We can observe that most of the beads are accumulated near the active conductor in the downstream side.

The dependency of the tagged-cell ratio, γ , on the actuation parameters, α and St , is slightly different from that of λ_1 , as shown in Figure 10. Tagging takes place even when λ_1 is negative, e.g., in the case of $\alpha = 3.48$ and $St = 1.0$. On the other hand, there are cases where the tagging is not frequent despite a high value of λ_1 , e.g., the case of $\alpha = 1.0$ and $St = 1.4$. The positions of beads in the latter case (i.e., $\alpha = 1.0$ and

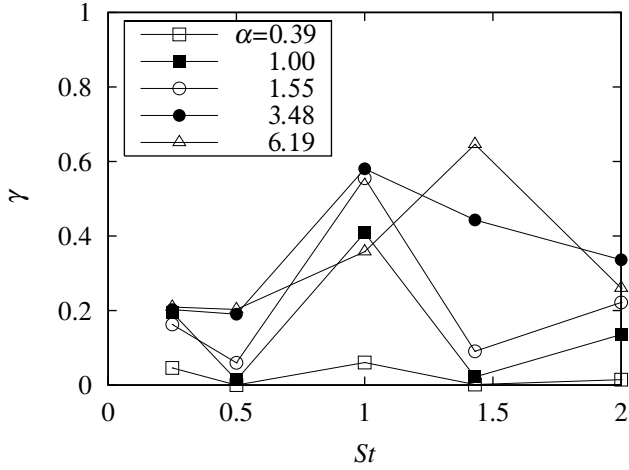


FIG. 10. Dependency of the tagged-cell ratio, γ , on the actuation parameters, α and St .

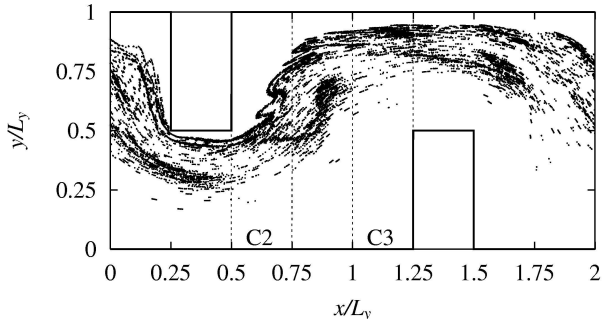


FIG. 11. Positions of magnetic beads at $\alpha = 1.0$ and $St = 1.4$ (Phase III).

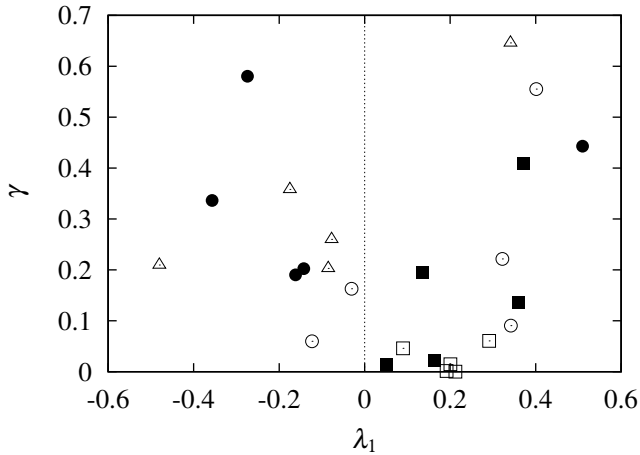


FIG. 12. Correlation between λ_1 and γ . Symbols represent α and are the same as those in Fig. 10.

$St = 1.4$) are plotted in Fig. 11. The mixing takes place only in the upper half in the conduit, where the cells are absent, and this causes the lower value of γ despite the higher value of λ_1 .

The relationship between λ_1 and γ is more clearly shown in

Fig. 12. Frequent tagging, i.e., a large value of γ , is associated with either a large positive value or a large negative value of λ . The large value of γ associated with $\lambda_1 > 0$ is simply attributed to the mixing enhancement, whereas that with a $\lambda_1 < 0$ is due to the entrapment of beads near the conductors, as has been observed in Fig. 9.

These two mechanisms are more clearly illustrated in Fig. 10, in which the positions of first contact between a cell and a magnetic bead are plotted. In Fig. 10a, (the case of $\lambda_1 > 0$) the contacts take place in the lower half of the conduit, where the cells are flowing. In Fig. 10b, (the case of $\lambda_1 < 0$) the most of contacts occurs around $(x/L_y, y/L_y) = (1, 0.5)$, where the magnetic beads are trapped by the strong magnetic force. A noteworthy observation is that the cell-tagging is almost completed within two mixer units ($0 \leq x/L_y \leq 4$).

B. Three-dimensional simulation

Three-dimensional simulations has also been made. The dimension of the conduit is $(L_x, L_y, L_z) = (320 \mu\text{m}, 160 \mu\text{m}, 35 \mu\text{m})$. The bulk Reynolds number is $Re_b = 0.025$. These parameters are the same as those in the experiment.⁸ The numbers of computational grids are 64, 32 and 16 in the x , y and z directions, respectively. Simulation is repeated with $St = 1.0$ and different values of α . However, in all test cases, all the beads sank toward the bottom wall and mostly accumulated near the conductors.

This is natural because both the magnetic and gravitational forces work downward, and there is no upward-driving force considered in the simulation. In the experiment by Suzuki et al.,⁸ the magnetic beads seem to flow without such a significant accumulation. Therefore, we may have missed to account for some upward forces in the present simulation.

A possible candidate for the upward force is the lift force. Under the present conditions, the Stokes length scale, $L_S = \nu/u_{max}$, and the Saffman length scale, $L_G = \sqrt{\nu/|(\partial u_i/\partial x_j)|}$, are estimated as $L_S \simeq 2 \times 10^{-3}$ m and $L_G \simeq 1 \times 10^{-4}$ m, respectively. Therefore, wherever a particle is located in the conduit ($L_z = 3.5 \times 10^{-5}$ m), the distance between the particle and the wall, l , is much less than $\min(L_S, L_G)$. According to the criteria proposed by Wang et al.,¹¹ the optimum expression of the lift force under the condition of $l \ll \min(L_S, L_G)$ is that by Cherukat and McLaughlin,¹² which includes both the shear and wall-induced lift forces. This lift force works upward when the magnetic beads are attracted toward the upstream direction. However, its magnitude is estimated as only one tenth of the gravitational force under the present conditions.

V. CONCLUSIONS

We have numerically investigated the mixing enhancement of magnetic beads and cells in a micro immunomagnetic mixer of Suzuki et al.⁸ The two-dimensional simulation clarifies a set of parameters which increase the largest Lyapunov

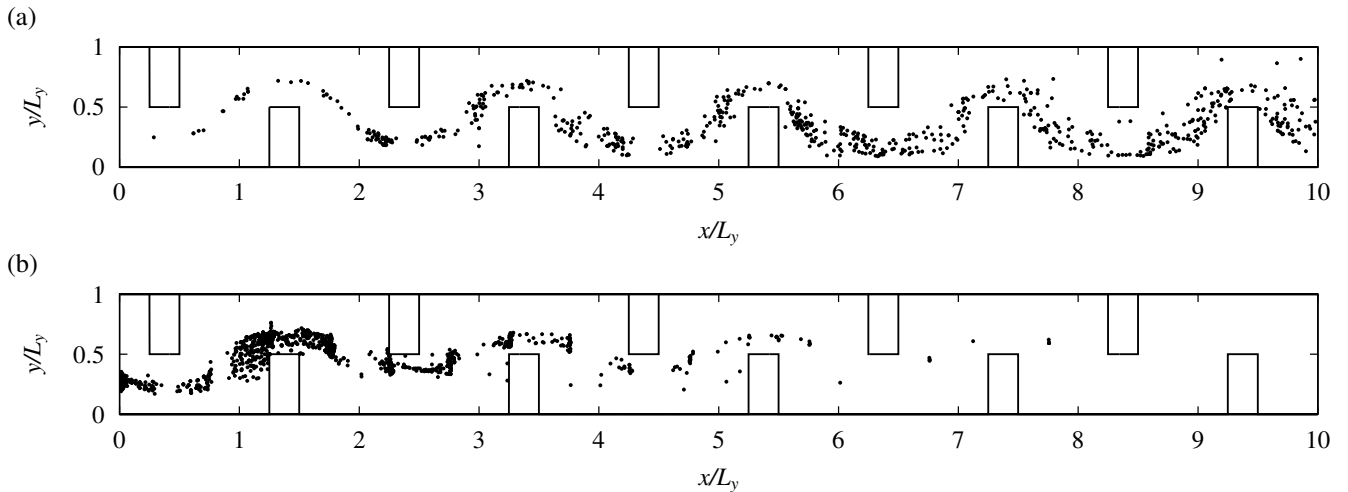


FIG. 13. Positions of the first contact between cells and magnetic beads: (a) $\alpha = 1.0$, $St = 1.0$; (b) $\alpha = 6.2$, $St = 1.0$.

exponent and the number of cells tagged by the immunomagnetic beads.

The simulation results reveal two different mechanisms for the enhancement of cell-tagging by the immunomagnetic beads: (1) the chaotic mixing, and (2) the entrapment of beads near the conductors. The former mechanism appears when the Strouhal number, defined based on the frequency of magnetic actuation and the conductor spacing, is unity and the terminal velocity of the beads due to the magnetic force is comparable to the bulk mean velocity of the fluid. The latter mechanism appears when the magnetic force is stronger. Since the cell-tagging is almost completed within one or two mixer units from the inlet, adoption of this operation mode has a merit in reducing the size of mixing device, if relatively large power consumption is allowed.

For three-dimensional simulations, there remains a critical issue of missing upward force.

ACKNOWLEDGMENTS

The authors are grateful to Dr. H. Suzuki (IIS, The Univ. of Tokyo), Prof. Y. Suzuki and Prof. N. Shikazono (Department of Mechanical Engineering, The University of Tokyo) for helpful comments and fruitful discussions. This work was supported through the Grant-in-Aid for Scientific Research (S) by the Ministry of Education, Culture, Sports and Technology of Japan (MEXT). The first author (KF) was supported through the Grant-in-Aid for Young Scientists (B) by the MEXT.

- [2] J. Branebjerg, P. Gravesen, J. P. Krog, and C. R. Nielsen, "Fast mixing by lamination," In: Proc. Annu. Workshop on MEMS (1996), pp. 441-446.
- [3] D. J., Beebe, R. J. Adrian, M. G. Olsen, M. A. Stremmer, H. Aref, and B. H. Jo., "Passive mixing in microchannels: fabrication and flow experiments," *Med. Ind.* **2**, 343-348 (2001).
- [4] W.-H. Tan, Y. Suzuki, N. Kasagi, N. Shikazono, K. Furukawa, and T. Ushida, "Development of novel micro mixer and its application to μ -immunomagnetic cell sorter," In: Proc. Micro TAS 2004, Malmö, Sweden (2004).
- [5] M. Volpert, C. D. Meinhart, I. Mezić, and M. Dahelh, "Modeling and numerical analysis of mixing in an actively controlled micromixer," In: Proc. 1st Int. Conf. on Heat Transfer, Fluid Mechanics, and Thermodynamics, Kruger Park, South Africa (2002).
- [6] X. Niu and Y. K. Lee, "Efficient spatial-temporal chaotic mixing in microchannels," *J. Micromech. Microeng.* **13**, 454-462 (2003).
- [7] J. Deval, P. Tabeling, and C.-M. Ho "A dielectrophoretic chaotic mixer," In: Proc. IEEE Int. Conf. MEMS 02 (2002), pp. 36-39.
- [8] H. Suzuki, C.-M. Ho, and N. Kasagi, "A chaotic mixer for magnetic bead-based micro cell sorter," *J. Microelectromech. Sys.* (2004, to appear).
- [9] J. M. Ottino, *The Kinematics of Mixing: stretching, Chaos, and Transport* (Cambridge University Press, New York, 1989).
- [10] J. C. Sprott, *Chaos and Time-Series Analysis* (Oxford University Press, 2003), pp.116-117.
- [11] Q. Wang, K. D. Squires, M. Chen, and J. B. McLaughlin, "On the role of the lift force in turbulence simulations of particle deposition," *Int. J. Multiphase Flow* **23**, 749-763 (1997).
- [12] P. Cherukat and J. B. McLaughlin, "The inertial lift on a rigid sphere in a linear shear flow," *J. Fluid Mech.* **263**, 1-18 (1994).

-
- [1] J. J. Chalmers, M. Zborowski, L. Sun, and L. Moore, "Flow through immunomagnetic cell separation," *Biotechnol. Prog.* **14**, 141-148 (1998).